Earth and Planetary Science Letters 489 (2018) 59–71

Contents lists available at ScienceDirect

Earth and Planetary Science Letters

www.elsevier.com/locate/epsl

Carbonate-platform response to the Toarcian Oceanic Anoxic Event in the southern hemisphere: Implications for climatic change and biotic platform demise

Zhong Han [a], Xiumian Hu [a,*], David B. Kemp [b], Juan Li [a]

[a] State Key Laboratory of Mineral Deposit Research, School of Earth Sciences and Engineering, Nanjing University, Nanjing 210023, China
[b] School of Geosciences, University of Aberdeen, Old Aberdeen AB24 3UE, UK

ARTICLE INFO

Article history:
Received 29 August 2017
Received in revised form 10 February 2018
Accepted 12 February 2018
Available online xxxx
Editor: D. Vance

Keywords:
Toarcian Oceanic Anoxic Event
Tibetan Himalaya
carbon isotopes
storm deposits
carbonate platform
southern hemisphere

ABSTRACT

The Toarcian Oceanic Anoxic Event (T-OAE, ~183 Ma) was a profound short-term environmental perturbation associated with the large-scale release of ^{13}C-depleted carbon into the global ocean–atmosphere system, which resulted in a significant negative carbon-isotope excursion (CIE). The general lack of characteristic T-OAE records outside of the northern hemisphere means that the precise environmental effects and significance of this event are uncertain. Many biotic carbonate platforms of the northern hemisphere western Tethys drowned or shifted to non-skeletal platforms during the early Toarcian. However, southern hemisphere records of Toarcian carbonate platforms are rare, and thus the extent and significance of biotic platform demise during the T-OAE is unclear. Here we present high-resolution geochemical and sedimentological data across two Pliensbachian–Toarcian shallow-water carbonate-platform sections exposed in the Tibetan Himalaya. These sections were located paleogeographically on the open southeastern tropical Tethyan margin in the southern hemisphere. The T-OAE in the Tibetan Himalaya is marked by a negative CIE in organic matter. Our sedimentological analysis of the two sections reveals an abundance of storm deposits within the T-OAE interval, which emphasizes a close link between warming and tropical storms during the T-OAE event, in line with evidence recently provided from western Tethyan sections of the northern hemisphere. In addition, our analysis also reveals extensive biotic carbonate-platform demise by drowning or changing to non-skeletal carbonates coincident with the onset of the CIE. Taken together, our results suggest that rapid and pervasive seawater warming in response to carbon release likely played a significant role in sudden biotic carbonate platform demise, and suppression/postponement of biotic platform re-development along the whole tropical/subtropical Tethyan margin.

1. Introduction

The early Toarcian Oceanic Anoxic Event (T-OAE, ~183 Ma) was characterized by abrupt global warming, enhanced weathering rates, expansion of anoxic conditions, and the worldwide accumulation of organic-rich sediments (e.g., Jenkyns, 1988, 2010; Cohen et al., 2004; Pearce et al., 2008; Dera et al., 2011; Brazier et al., 2015; Fu et al., 2016). It is characteristically marked by a negative carbon isotope (δ^{13}C) excursion (CIE) with an amplitude of ~3–8‰, which typically interrupts a longer-term positive excursion attributable to the global increase in organic carbon burial. The CIE has been recognized in bulk organic carbon, bulk carbonate, fossil wood and phytoclasts. In some studies, the shift to minimum δ^{13}C values has been shown to occur in discrete, periodic steps (Kemp et al., 2005; Hesselbo et al., 2007; Hermoso et al., 2009, 2012; Hesselbo and Pieńkowski, 2011; Them et al., 2017). Two hypotheses have been put forward to explain the CIE: (i) methane hydrate dissociation from marine sediments and consequent release of ^{12}C (e.g., Hesselbo et al., 2000; Kemp et al., 2005); (ii) thermogenic emission of ^{12}C induced by the intrusive emplacement of Karoo-Ferrar sills in organic-rich mudrocks (e.g., McElwain et al., 2005).

Although the T-OAE has been well documented in the western Tethys and Boreal realms (i.e., Europe, e.g., Kemp et al., 2005; Hesselbo et al., 2007; Hermoso et al., 2009, 2012), fewer studies have been conducted elsewhere. Notable exceptions are recent studies from the NE Tethys (Fu et al., 2016), NW, central and NE Panthalassa (Caruthers et al., 2011; Gröcke et al., 2011; Kemp and Izumi, 2014), and the Sichuan Lake Basin, China (Xu et al., 2017).

* Corresponding author.
E-mail address: huxm@nju.edu.cn (X. Hu).

https://doi.org/10.1016/j.epsl.2018.02.017
0012-821X/

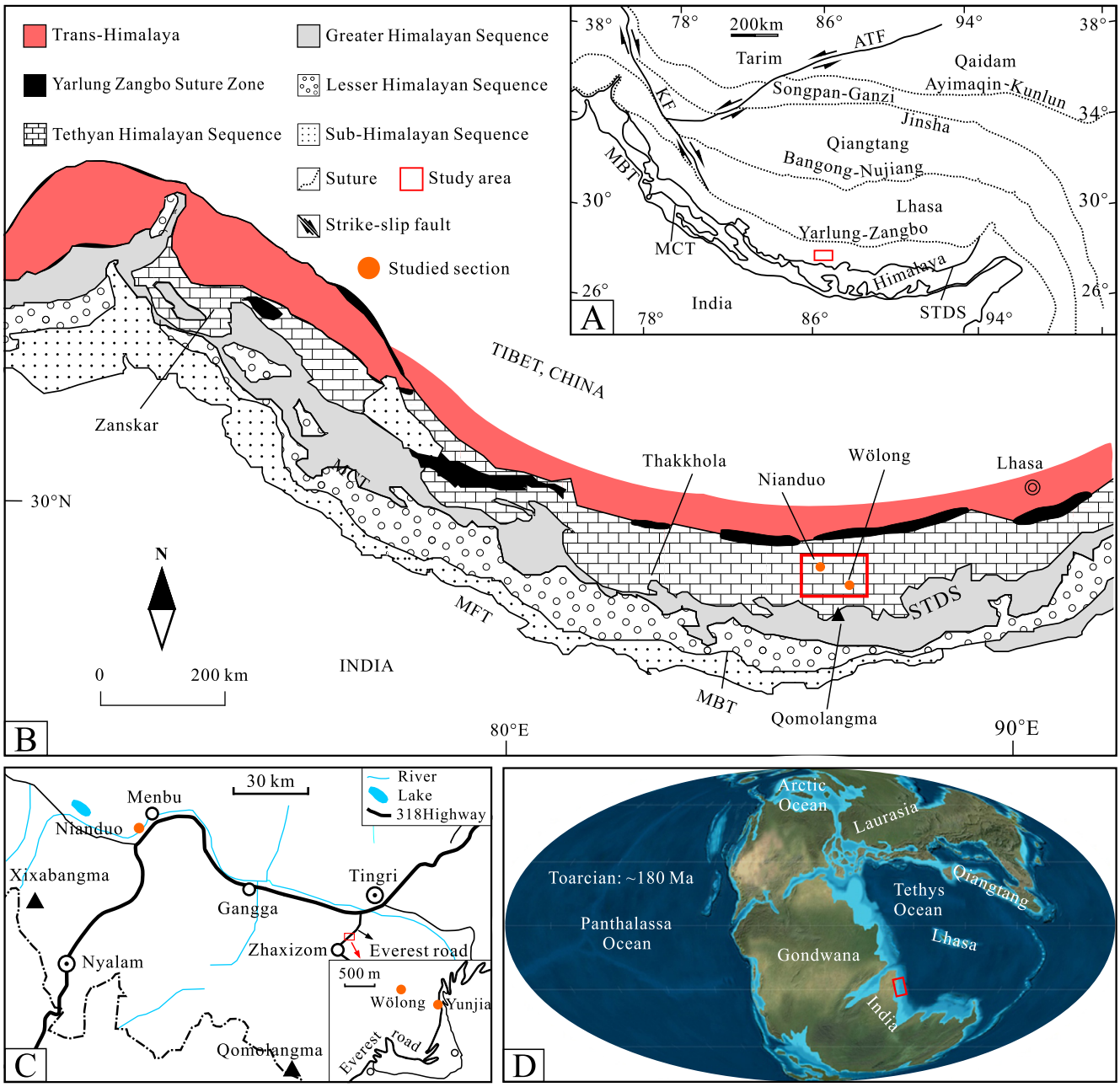

Fig. 1. (A) Simplified tectonic map of the Tibetan Plateau showing the major blocks and sutures. MFT: Main Frontal Thrust; MBT: Main Boundary Thrust; MCT: Main Central Thrust; STDS: Southern Tibetan Detachment System; ATF: Alty Tagh Fault; KF: Karakorum Fault. (B) Geological sketch map of the Himalayas showing the studied areas, modified after Gansser (1964). (C) Road map showing detailed location of three Toarcian sections: Wölong, Nianduo and Yunjia. (D) Global palaeogeographic setting during the Toarcian showing the northern Indian continental margin (adapted from Ron Blakey, http://jan.ucc.nau.edu/~rcb7/).

In the southern hemisphere, however, the T-OAE has been reported only from the Neuquén Basin, Argentina, which is a restricted back-arc rift basin formed during the Mesozoic (Al-Suwaidi et al., 2010, 2016). Therefore, no record of the T-OAE has been reported from an open-ocean setting in the southern hemisphere. Consequently, there is uncertainty as to whether the Toarcian CIE and corresponding environmental perturbations affected the southern hemisphere in the same way as the northern hemisphere. This has implications for assessing the severity, importance, and casual mechanism(s) of the event.

At the onset of the T-OAE, extensive demise of biotic carbonate platforms occurred in the western Tethys, attributed variously to the effects of falling carbonate production, tectonics, eustasy, increased nutrient levels, or oceanic acidification (Woodfine et al., 2008; Lachkar et al., 2009; Merino-Tomé et al., 2012; Trecalli et al., 2012; Sabatino et al., 2013). However, the study of the relationship between the T-OAE and carbonate-platform evolution has thus far been restricted to the southern margins of western Tethys at low latitudes of the northern hemisphere. Consequently, only a localized understanding of carbonate-platform responses to the T-OAE has hitherto been gained, and the factors that triggered the demise of biotic platforms and delayed their recovery until well after the event are still uncertain and need to be better constrained.

In this paper, we present sedimentological and geochemical data across two uppermost Pliensbachian to lower Toarcian shallow-marine carbonate platform successions exposed in the Tibetan Himalaya, deposited at a low latitude (~21.8°S to ~26.1°S) in the southern hemisphere (Fig. 1A; Huang et al., 2015). We as-

sess the environmental evolution of these platforms through the T-OAE, and discuss the possible global/regional factors controlling platform evolution and sedimentology along the Tethyan margin.

2. Geological setting

2.1. Tectonic setting

The Tethyan Himalayan Sequence, located between the Indus-Yarlung Zangbo Suture Zone to the north and the Greater Himalayan Sequence to the south (Fig. 1A and B; Gansser, 1964), consists mainly of Proterozoic to Eocene carbonate and siliciclastic sedimentary rocks that originally represented the northern margin deposits of the Indian subcontinent (Fig. 1D; Liu and Einsele, 1994; Jadoul et al., 1998; Sciunnach and Garzanti, 2012). This unit was traditionally subdivided into southern and northern zones. The southern zone is dominated by Lower Paleozoic to Lower Eocene shallow-water carbonates and terrigenous rocks (Liu and Einsele, 1994; Jadoul et al., 1998; Sciunnach and Garzanti, 2012), whereas the northern zone is characterized by Mesozoic to Paleocene deep-water slope and rise sediments (Liu and Einsele, 1994). During the Early Jurassic, the Tethyan Himalaya migrated into the southern tropical/subtropical belt, and carbonate deposits gradually became extensive in the southern zone, forming the Kioto carbonate platform (Jadoul et al., 1998; Sciunnach and Garzanti, 2012; Huang et al., 2015).

2.2. Stratigraphy

The Nianduo section in the Nyalam area and the Wölong section in the Tingri area are located in the Tethyan Himalaya on the Kioto carbonate platform (Fig. 1B). Both sections have a continuously exposed marine sedimentary succession ranging from the upper Lower Jurassic Pupuga Formation to the lower Middle Jurassic Nieniexiongla Formation (Fig. 2A–D). The Pupuga Formation represents a shallow-water carbonate platform dominated by grainstones/packstones deposited under high-energy conditions with occasional influxes of terrigenous material. The lower-middle Pupuga Formation in both Tingri and Nyalam areas yields abundant and diversified benthic foraminifera including *Haurania deserta*, *Orbitopsella praecursor*, *Palaeomayncina termieri*, *Amijiella amiji, Cyclorbitopsella tibetica*, *Ammobaculites sp.*, *Lituosepta cf. compressa*, *Pseudocyclammina cf. liasica* (Jadoul et al., 1998; Wignall et al., 2006). These foraminiferal assemblages of the Tibetan Himalaya are similar to those observed in the Liassic carbonate platforms of the SW Tethyan margin in the northern hemisphere, and indicate a late Sinemurian–late Pliensbachian age (BouDagher-Fadel, 2008). In the upper Pupuga Formation, two intervals enriched in *Lithiotis* bivalves respectively occur ~20–30 m and ~3–4 m below the boundary with the overlying Nieniexiongla Formation in both the Nianduo and Wölong sections (Figs. 3 and 4). *Lithiotis* bivalves are found in carbonate platforms throughout the tropical Tethys and Panthalassa, where they are limited to strata of late Pliensbachian to early Toarcian age (Fraser et al., 2004; Franceschi et al., 2014; Bodin et al., 2016). The overlying Nieniexiongla Formation represents a middle/outer carbonate ramp environment, and is characterized by mudstones deposited under low-energy conditions intercalated with abundant coarse-grained beds (Han et al., 2016). In the lower Nieniexiongla Formation, ammonites (*Polyplectus discoides*, *Dumortieria sp.*, *Phymatoceras cf. crasstcosta*) collected in thin-bedded mudstones near the Nianduo section were assigned to the *bifrons-levesquei* zones of the middle-late Toarcian (Fig. 3; Yin, 2010). The upper part of this unit in the Wölong section yields ammnonites (*Leptosphinctes sp.*) suggestive of a Bajocian age (Jadoul et al., 1998). In addition to these biostratigraphic constraints, further important information on the age of the studied stratigraphy can be derived from available stable sulfur isotope ($\delta^{34}S$) stratigraphy (Newton et al., 2011). Based on the *lituolid* foraminifera and *Lithiotis* bivalves, the studied sections can be readily correlated with the nearby Yunjia section (~500 m away from the Wölong section, Fig. 1C). Newton et al. (2011) suggested that a marked shift in $\delta^{34}S$ data in the Yunjia section close to the Pupuga–Nieniexiongla boundary can be correlated with a similar shift in the biostratigraphically well-constrained Yorkshire (UK) section. Based on this correlation, the Pupuga–Nieniexiongla transitional interval is most probably coeval with the upper *tenuicostatum*–lower *falciferum* ammonite Zone boundary in Europe, and thus of early Toarcian age.

3. Material and methods

Rock samples were collected from the Nianduo section (28°40′52″N, 86°08′7″E) of Nyalam County and the Wölong section (28°29′2″N, 87°02′3″E) of Tingri County in the Tibetan Himalaya (Fig. 1B and C). Samples were collected with an average spacing of 1 m, reduced to ~0.2–0.3 m in the Nianduo section and 0.1–0.2 m in the Wölong section across the Pupuga–Nieniexiongla stratigraphic transition.

A total of 132 samples from the Nianduo section and 124 samples from the Wölong section were analyzed for organic carbon-isotope composition ($\delta^{13}C_{org}$) at the SINOPEC Wuxi Research Institute of Petroleum Geology. Powdered samples were treated with 2N HCl at 80 °C for at least 3 hours to remove carbonate, and were then washed with distilled water to remove residual HCl. Organic carbon-isotope analyses were performed on dried samples using a Finnigan MAT 253 mass spectrometer, with an instrumental standard deviation of ±0.1‰. Isotopic measurements were calibrated to Chinese national standard charcoal sample GBW04407 ($\delta^{13}C_{VPDB} = -22.43‰ \pm 0.07‰$). Results were reported in standard δ-notation relative to the Vienna Peedee Belemnite (VPDB) standard. To supplement our $\delta^{13}C_{org}$ data, $\delta^{13}C$ and $\delta^{18}O$ of bulk carbonate were measured on 98 samples across the Pupuga–Nieniexiongla boundary interval in the Nianduo section using a Finnigan MAT 252 isotope ratio mass spectrometer at the State Key Laboratory of Marine Geology at Tongji University. The isotope results of $\delta^{13}C_{carb}$ and $\delta^{18}O_{carb}$ were corrected to VPDB standard, with analytical uncertainties of ±0.06‰ and ±0.08‰, respectively.

Total organic carbon (TOC) analysis was performed on 69 samples, parallel to the $\delta^{13}C_{carb}$ samples, across the Pupuga–Nieniexiongla boundary interval in the Nianduo section using a Vario Cube CN elemental analyzer (Elementar, Germany) at the State Key Laboratory of Marine Geology of Tongji University. Prior to analysis, these samples were treated with 10% HCl for at least 24 h to remove inorganic carbon. Titanium concentrations was determined on 53 powdered samples from the Nianduo section using an Olympus Delta Premium handheld XRF (hhXRF) instrument at the University of Aberdeen. The calibration error (uncertainty) of Ti measurements is better than 0.04%. Reproducibility, based on repeat measurement of a standard, was better than 0.009% (1 s.d., 2.36% relative s.d.).

4. Results

4.1. Geochemical data

4.1.1. Isotope geochemistry

Carbon- and oxygen-isotope data are plotted stratigraphically in Fig. 3 for the Nianduo section and in Fig. 4 for the Wölong section. In the Nianduo section, a negative CIE of ~−2.5‰ is recorded in organic matter (−0.3 to 28.4 m; Fig. 3). This CIE starts at the topmost Pupuga Formation, just above the top of the *Lithiotis*-rich interval. $\delta^{13}C_{org}$ values are variable between −0.3 m and ~16 m

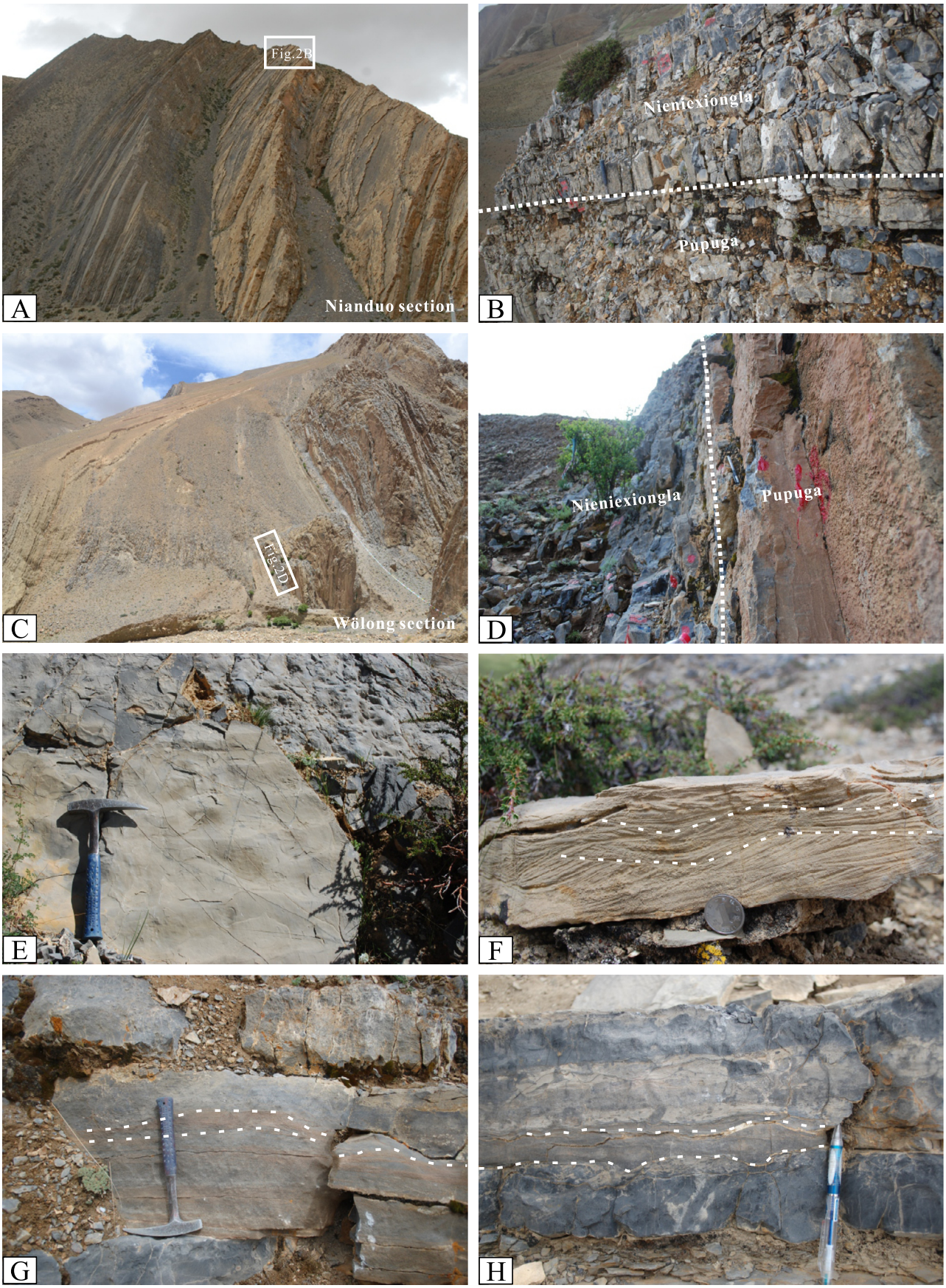

Fig. 2. Field photographs of the studied sections and storm deposits within the T-OAE interval. (A and B) Nianduo section and (C and D) Wölong section showing the detailed abrupt facies change at the Pupuga–Nieniexiongla boundary (dashed white line) within the Pliensbachian–Toarcian carbonate successions. (E) Ripple marks. (F) Storm beds with HCS/SCS. (G) Sandy beds within mudstones showing weak HCS. (H) V-shaped gutter casts filled with mixed coarse carbonate and terrestrial grains showing HCS/SCS.

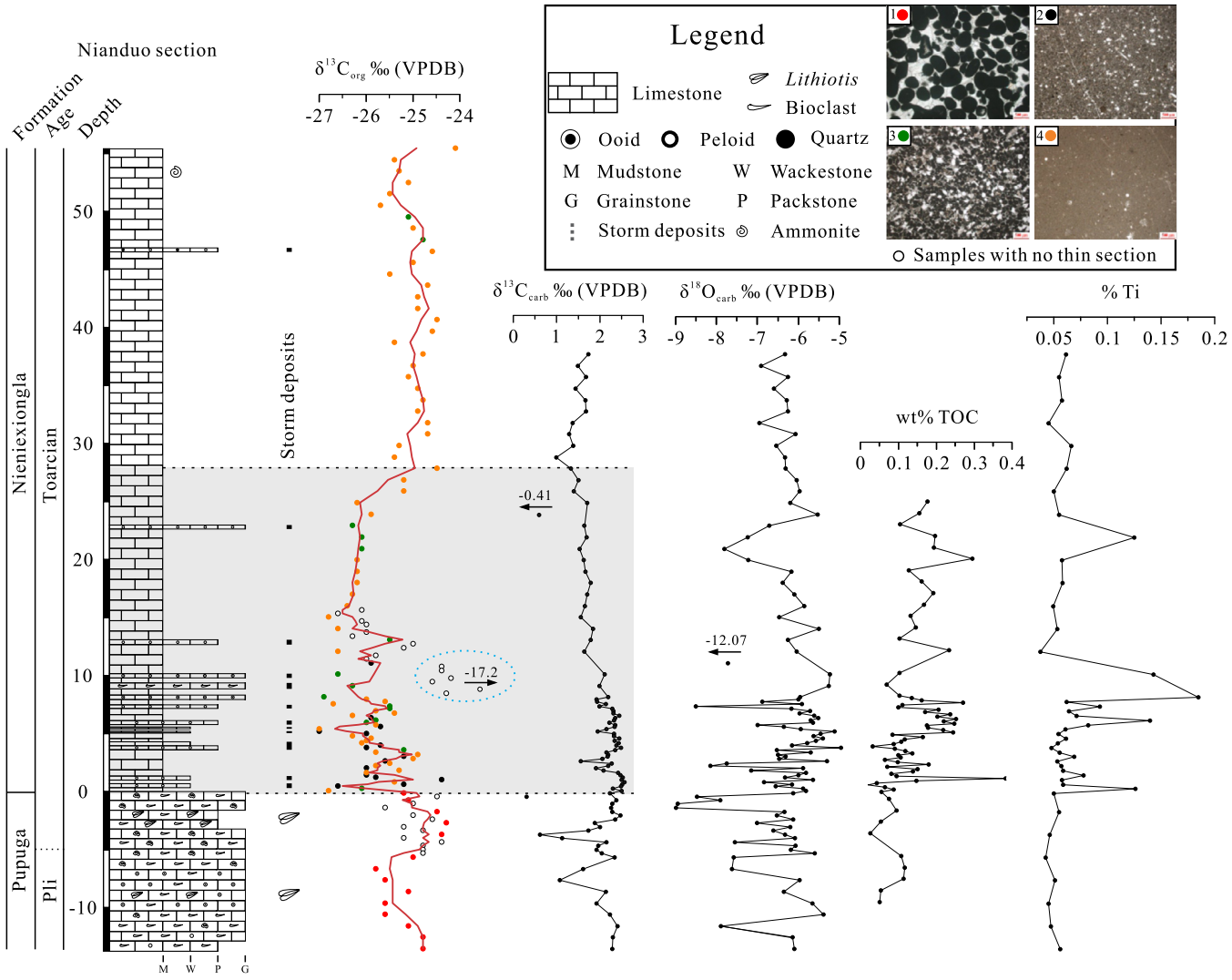

Fig. 3. Nianduo section shows stratigraphic distribution of organic carbon isotopes ($\delta^{13}C_{org}$), carbonate carbon and oxygen isotopes ($\delta^{13}C_{carb}$ and $\delta^{18}O_{carb}$), total organic carbon (TOC), and Ti. The $\delta^{13}C_{org}$ data are plotted as different colors based on the facies observed in thin sections of the analyzed samples (microfacies 1–4 as shown in legend). Microfacies are: 1 (red datapoints): Oolitic grainstone; 2 (black datapoints): Fine-grained peloidal packstone; 3 (green datapoints): Sandy peloidal packstone/grainstone; 4 (orange datapoints): Mudstone. The red line through the data is the 3-point moving average. Note that this averaging omits the 6 datapoints (circled with blue dashed ellipse) at ~10 m height that lie well away from the rest of the data and are likely influenced by terrestrial input (see main text for details). Note the distribution of storm beds and relative abundance of storm beds within the CIE interval between ~0 and ~10 m. (For interpretation of the colors in the figure(s), the reader is referred to the web version of this article.)

during the overall shift to minimum values. $\delta^{13}C_{carb}$ data primarily range between 1‰ and 2.5‰, and show an overall negative trend beginning shortly after the Pupuga–Nieniexiongla boundary (~0 m) and extending to ~30 m, with a small magnitude of ~−1.5‰. However, $\delta^{13}C_{carb}$ data do not show the same profile as the $\delta^{13}C_{org}$ data (Fig. 3). The corresponding oxygen-isotope data mainly range from −8 to −5‰, with an average value of −6.4‰.

Compared to the Nianduo section, $\delta^{13}C_{org}$ data in the Wölong section do not show a decreasing trend close to the Pupuga–Nieniexiongla boundary (Fig. 4). A broad negative CIE of ~−2.5‰ is, however, apparent higher up in the section between ~8 m and ~30 m. The recovery profile of this excursion between ~15 m and ~30 m is similar to the recovery profile of the $\delta^{13}C_{org}$ data between ~15 m and ~30 m in the Nianduo section.

4.1.2. TOC and elemental content

TOC values from the Nianduo section range from 0.05 to 0.3 wt.%, with an average value of 0.14 wt.% (Fig. 3). An increase in TOC values occurs shortly after the onset of the CIE between ~0 m and ~8 m. Ti abundance in the Nianduo section is plotted in Fig. 3 and primarily ranges between 0.05% and 0.15%, with an average value of 0.069%.

4.2. Sedimentological observations

As noted above, and previously by Han et al. (2016), platform-top grainstones deposited under high-energy conditions of the Pupuga Formation are abruptly overlain by middle/outer ramp mudstones reflecting low-energy conditions of the Nieniexiongla Formation in the Nianduo and Wölong sections (0 m datum in both sections). The interval immediately above this flooding surface in both the Nianduo and Wölong sections is characterized by the common occurrence of coarse-grained beds, e.g., rudstones, floatstones, siltstones, oolitic grainstones, and peloidal packstones/wackestones (Han et al., 2016; Figs. 3 and 4). These intervals show abundant and diverse sedimentary structures such as wave ripples (Fig. 2E) and small-scale hummocky and swaley cross-stratification (HCS and SCS; Fig. 2F). Some sandy beds within mudstones show weak HCS individually (Fig. 2G) or just above the U/V-shaped gutter casts (Fig. 2H). In addition, other sedimentary

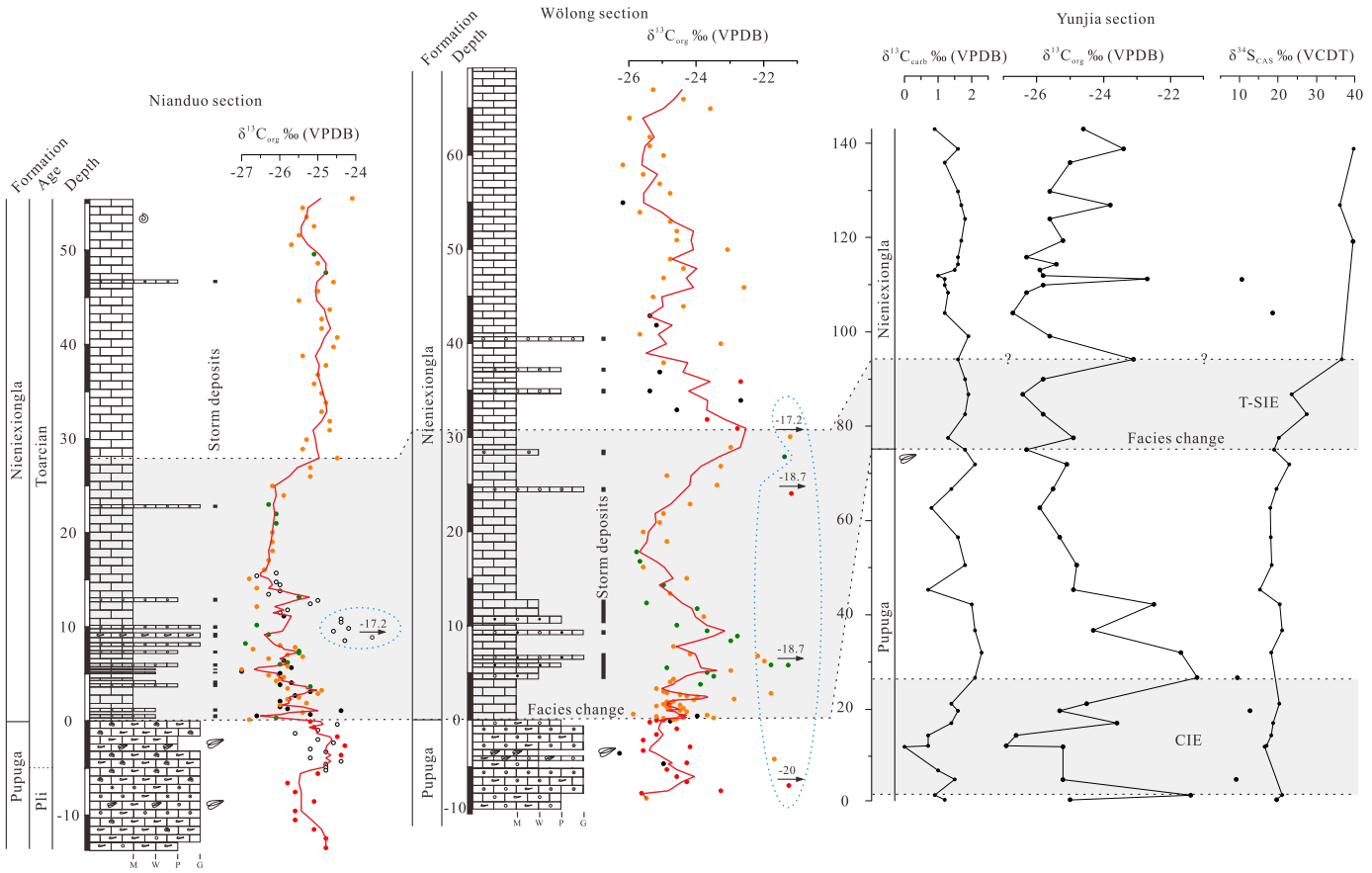

Fig. 4. Correlation between the Tibetan sections based on the position of the top *Lithiotis* horizon and the Pupuga–Nieniexiongla boundary, i.e., the Toarcian maximum flooding surface, facies change (Han et al., 2016) and extinction level (Wignall et al., 2006), and carbon- and sulfur-isotope stratigraphy. $\delta^{13}C_{org}$ datapoint color coding is based on the microfacies, as in Fig. 3. Red line through the $\delta^{13}C_{org}$ data in both the Nianduo and Wölong sections is the 3-point moving average. Moving average for Nianduo section as in Fig. 3. For the Wölong section, 9 anomalously high $\delta^{13}C_{org}$ values (in blue dashed ellipse) are omitted from the moving average. These are likely influenced by terrestrial input (see main text for details). The Yunjia section shows the stratigraphic distribution of organic and carbonate carbon-isotope data ($\delta^{13}C_{org}$ and $\delta^{13}C_{carb}$), and carbonate-associated sulfate (CAS) isotope data ($\delta^{34}S_{CAS}$) (data from Newton et al., 2011 and Wignall et al., 2006). T-SIE: Early Toarcian sulfur-isotope excursion. Grey shading between ~2 and ~27 m in the Yunjia section delineates CIE recognized in Wignall et al. (2006), see main text for details.

structures, e.g., parallel laminations, climbing ripples, graded bedding and sharp erosive bases, are also readily observed both at outcrop and in microfacies (Han et al., 2016). These coarse-grained beds and related structures are particularly concentrated in the Nianduo section between ~0 m and ~12 m, coincident with the overall shift to minimum $\delta^{13}C_{org}$ values. In the Wölong section, they are also concentrated close to the base of the Nieniexiongla Formation.

5. Discussion

5.1. Diagenetic and source effects on carbon-isotope data

The early Toarcian negative CIE has been widely recorded in a range of marine environments, including shallow-water carbonate platforms (Kemp et al., 2005; Hesselbo et al., 2007; Woodfine et al., 2008; Trecalli et al., 2012; Sabatino et al., 2013; Them et al., 2017). However, high-energy deposits on shallow-water platforms are readily influenced by freshwater diagenesis or organic matter source changes (Oehlert and Swart, 2014; Suan et al., 2015). The measured $\delta^{18}O$ values ($>-10‰$) in the Nianduo section, coupled with the absence of any correlation between $\delta^{18}O$ and $\delta^{13}C_{carb}$ ($R^2 = 0.005$, Fig. 5A), suggests limited diagenetic influence on the $\delta^{13}C_{carb}$ data (Brasier et al., 1990; Kaufman and Knoll, 1995). The decoupled $\delta^{13}C_{org}$ and $\delta^{13}C_{carb}$ relationship ($R^2 = 0.023$, Fig. 5B) possibly indicates evidence for diagenetic alteration (e.g., Knoll et al., 1986, see also, however, Oehlert and Swart, 2014). Nevertheless, the overall pattern of $\delta^{13}C_{org}$ changes in the Nianduo section is comparable to that recognized from well-preserved T-OAE successions elsewhere (e.g., Kemp et al., 2005; Hesselbo et al., 2007; Hermoso et al., 2009, 2012; Sabatino et al., 2013, see discussion below), albeit with lower magnitude variations (Figs. 6 and 7). The range of $\delta^{13}C_{org}$ values from the Nianduo section broadly correspond to the coeval range known from the western Tethyan Apennine and High Atlas platforms (Trecalli et al., 2012; Bodin et al., 2016). Taken together, therefore, these observations suggest that the $\delta^{13}C_{org}$ signal form the Nianduo section is not significantly modified by diagenesis.

Given the abrupt facies change and appearance of coarse grained siliciclastic-rich beds at the upper Pupuga Formation to lower Nieniexiongla Formation boundary, we consider the possible influence of organic-matter source changes on our $\delta^{13}C_{org}$ data caused by microfacies variations and terrestrial input. To do this, we divided the lithologies of the Nianduo and Wölong sections into four characteristic microfacies based on grain type and/or size (Figs. 3 and 4). $\delta^{13}C_{org}$ data from each microfacies are shown on the stratigraphic log for the two sections (Figs. 3 and 4). In addition, Fig. 5C shows cross-plots between $\delta^{13}C_{org}$ from each microfacies in the Nianduo section and Ti, a proxy for detrital input (e.g., Kemp and Izumi, 2014). The data indicate that each microfacies type has a wide range of $\delta^{13}C_{org}$ values, and there is no clear relationship between microfacies and $\delta^{13}C_{org}$. Thus, the $\delta^{13}C_{org}$ values from the Tibetan sections are independent of changes of grain type and/or size. Overall, $\delta^{13}C_{org}$ varies independently of Ti

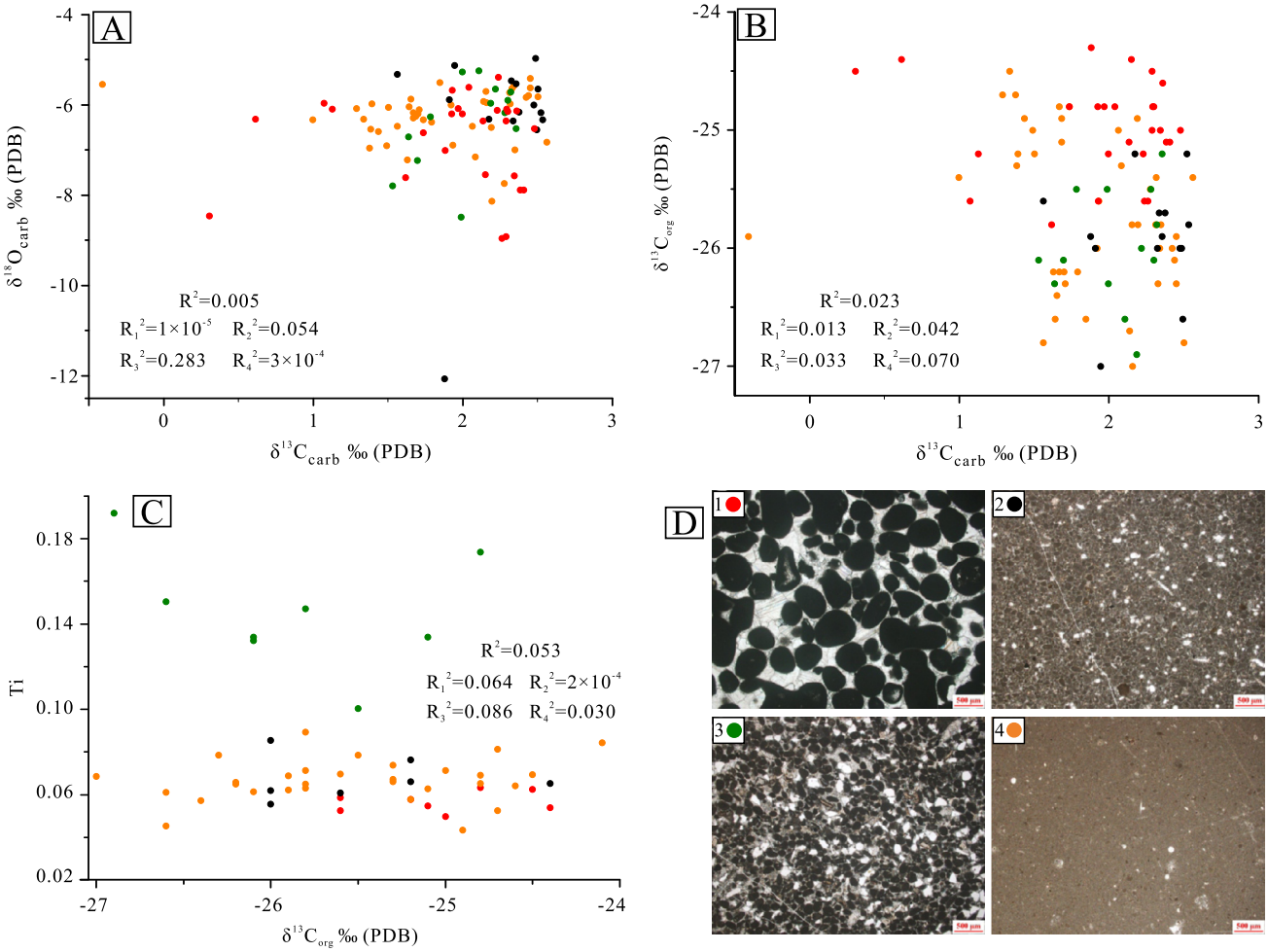

Fig. 5. Cross-plots of $\delta^{13}C_{carb}$–$\delta^{18}O_{carb}$ (A), $\delta^{13}C_{carb}$–$\delta^{13}C_{org}$ (B) and $\delta^{13}C_{org}$–Ti (C) within typical microfacies of the Nianduo section. (D) shows characteristic microfacies 1 to 4: 1 (red datapoints): Oolitic grainstone; 2 (black datapoints): Fine-grained peloidal packstone; 3 (green datapoints): Sandy peloidal packstone/grainstone; 4 (orange datapoints): Mudstone.

for each microfacies, and although microfacies 3 is typically associated with high Ti values (Fig. 5C), $\delta^{13}C_{org}$ values of microfacies 3 are variable and show no correlation with Ti. These observations further suggest that changes in detrital input, and thus possible changes in terrestrial organic matter flux, likely have a negligible influence on the observed changes in $\delta^{13}C_{org}$ in the Nianduo section. Nevertheless, we note that 6 samples with anomalously high $\delta^{13}C_{org}$ values at ~10 m height in the Nianduo section come predominantly from an interval of enhanced detrital input, as indicated by higher Ti values (Fig. 3). This observation may be ascribed to the fact that these specific samples have the most significant terrigenous influence, and are thus potentially more readily affected by organic matter source change, i.e., compositional mixing. Indeed, $\delta^{13}C_{org}$ in both sections may be sensitive to organic matter source changes given the conditions of extremely low TOC values (typically $<<$1%, Fig. 3). Therefore, we can reasonably infer that a few scattered and anomalously high $\delta^{13}C_{org}$ values from microfacies 1, 3 and 4 in the Wölong section may also be influenced by compositional mixing (Fig. 4).

5.2. The T-OAE record in the Tibetan Himalaya

As noted earlier, the overall $\delta^{13}C_{org}$ trend in the Nianduo section is comparable to that recognized from well-preserved T-OAE of siliciclastic and carbonate successions elsewhere (e.g., Kemp et al., 2005; Hesselbo et al., 2007; Hermoso et al., 2009, 2012; Trecalli et al., 2012; Sabatino et al., 2013; Figs. 6 and 7). The Tethyan Himalaya was a mature and tectonically quiescent passive margin of northern India, with smooth subsidence during the Jurassic (Sciunnach and Garzanti, 2012). Therefore, our studied Tibetan Himalayan sections can be readily correlated with each other on the basis of the characteristic top *Lithiotis* beds and associated flooding surfaces (Fig. 4). This correlation indicates that the onset of the $\delta^{13}C_{org}$ excursion of the Nianduo section is marked by environmental and biotic changes, i.e., a sharp facies change, benthic extinction level, development of dysoxic bottom waters (Wignall et al., 2006; Han et al., 2016) and TOC increase (Figs. 3 and 4). As noted in section 2.2, we attribute these marked changes to the onset of the T-OAE owing to the biostratigraphic age constraints in the sections, and because the onset of our new $\delta^{13}C_{org}$ excursion agrees well with the suggested correlation between the abrupt positive $\delta^{34}S$ excursion of the Yunjia section and the $\delta^{34}S$ excursion recorded across the T-OAE in Yorkshire, UK (Newton et al., 2011). Indeed, no other excursion in $\delta^{34}S$ of this magnitude is recognized elsewhere in the Jurassic (Gill et al., 2011). Some debate surrounding the age assignment of the Himalaya strata exists, however. Notably, the extremely high $\delta^{34}S$ values and anomalously low sulfate oxygen isotope values in the Yunjia section (Newton et al., 2011) suggest that the carbonate-associated sulfate $\delta^{34}S$ ($\delta^{34}S_{CAS}$) signal in this section might have been modified by diagenesis (Gill et al., 2011). However, a recent study shows that $\delta^{34}S_{CAS}$ can withstand burial diagenesis and reliably preserve a record of ambient seawater sulfate and early diagenetic redox processes (Fichtner et al., 2017). A further consideration is that a second, broad nega-

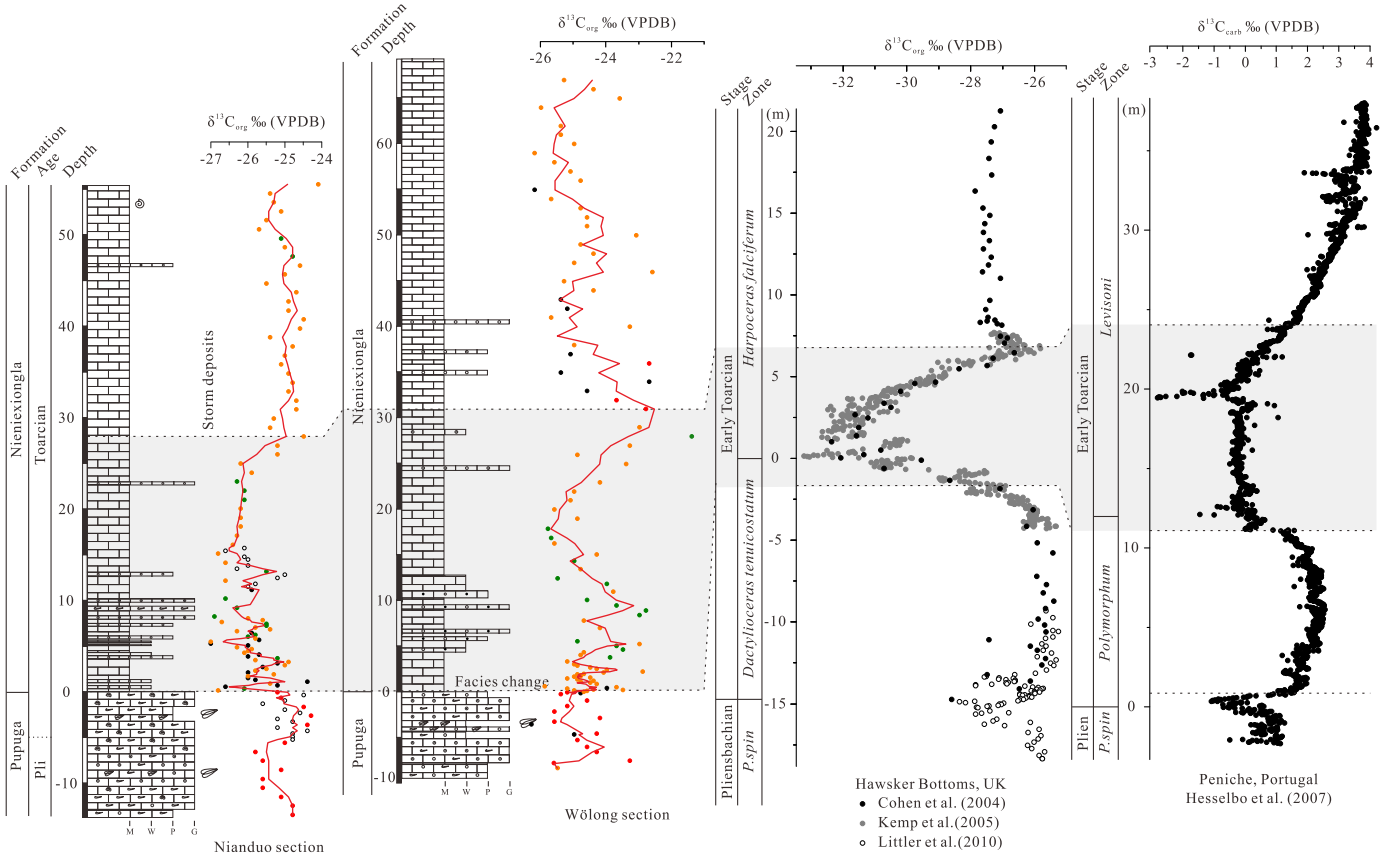

Fig. 6. Chemostratigraphic correlation of the Pliensbachian–Toarcian transition from the Tibetan sections in this study with sections from Europe (Hawsker Bottoms, UK; Cohen et al., 2004; Kemp et al., 2005; Littler et al., 2010, and Peniche, Portugal; Hesselbo et al., 2007). The profiles have been correlated using the onset and end of the carbon isotope excursions (CIEs). *P. spin* = *Pleuroceras spinatum*, Pl. = Pliensbachian. Note that the Wölong section does not show a clear CIE, see main text for details.

tive $\delta^{13}C$ CIE was reported in the bottom part of the Yunjia section (~2–27 m, shaded interval on Fig. 4), which was considered as the possible characteristic T-OAE excursion due to both its shape and the occurrence of rare calcareous nannofossils higher in the section (~88 m) that were constrained to an early mid-Aalenian age (Fig. 4; Wignall et al., 2006). Given these observations, the rapid $\delta^{34}S$ positive excursion above this $\delta^{13}C_{org}$ negative CIE could be regarded as a possible Aalenian event (Newton et al., 2011). Further combined with additional anomalously high $\delta^{13}C_{org}$ values (>−27‰) in the Tibetan Himalayan sections, Gill et al. (2011) also thought that the Tibetan $\delta^{34}S$ excursion could represent a stratigraphically higher event. However, the onset of this lower CIE in the Yunjia section is not marked by any environmental and biotic changes, and if this CIE was the T-OAE then the extinction level of the *Lithiotis* bivalves would be late Toarcian, which is considered unlikely (Newton et al., 2011). In addition, according to the available biostratigraphy and chemostratigraphy, we note that: 1) the CIE between ~2 and ~27 m occurs at a position in the *Orbitopsella* foraminifera-rich horizons (Wignall et al., 2006; Han et al., 2016), which most probably indicates a late Pliensbachian age (BouDagher-Fadel, 2008); 2) it is hard to reconcile the position of ostensible mid-Aalenian calcareous nanofossils found at the base of the Nieniexiongla Formation (12 m above the Pupuga–Nieniexiongla boundary) by Wignall et al. (2006) with the position of middle-late Toarcian ammonites found in the lower Nieniexiongla Formation by Yin (2010), and 3) as discussed in section 5.1, the absolute $\delta^{13}C_{org}$ values of the Tibetan sections broadly correspond to those of the western coeval carbonate platforms. Hence, the biostratigraphic and chemostratigraphic constraints here suggest that the age assignment of the Yunjia section by Wignall et al. (2006) is incorrect, and the Pupuga–Nieniexiongla transition does indeed correspond to the onset of the T-OAE.

The $\delta^{13}C_{org}$ trend of the Wölong section close to the onset of the T-OAE does not correspond well to that of the Nianduo section (Fig. 4). This difference could be due to hiatuses caused by subaerial exposure in the shallow platform environment. In addition, although the $\delta^{13}C_{carb}$ records in the Nianduo section overall show a negative CIE around −1.5‰, its shape and magnitude are significantly different from those of the typical T-OAE CIE elsewhere (e.g., Kemp et al., 2005; Hesselbo et al., 2007; Hermoso et al., 2009; Sabatino et al., 2013; Them et al., 2017). Such a phenomenon also occurs in the $\delta^{13}C_{carb}$ expression of the Toarcian CIE in several Toarcian shallow-water carbonate successions elsewhere (Woodfine et al., 2008; Trecalli et al., 2012). Moreover, in other marine settings, many coeval $\delta^{13}C_{carb}$ records in bulk carbonate and belemnites from western Tethys also do not show obvious negative CIE shapes/magnitudes that match with CIEs recorded in organic matter (e.g., Hesselbo et al., 2000; Jenkyns et al., 2002; van de Schootbrugge et al., 2005; Gill et al., 2011).

5.3. Intensified storm events and extreme warmth during the early Toarcian

A key feature of the Toarcian CIE interval in both the Nianduo and Wölong sections is the common occurrence of coarse-grained deposits and sedimentary structures associated with high-energy conditions within the otherwise low-energy carbonate ramp environment of the Nieniexiongla Formation (see 4.2, Figs. 3 and 4). HCS/SCS and wave rippled surfaces are important storm-generated sedimentary structures formed under oscillating wave

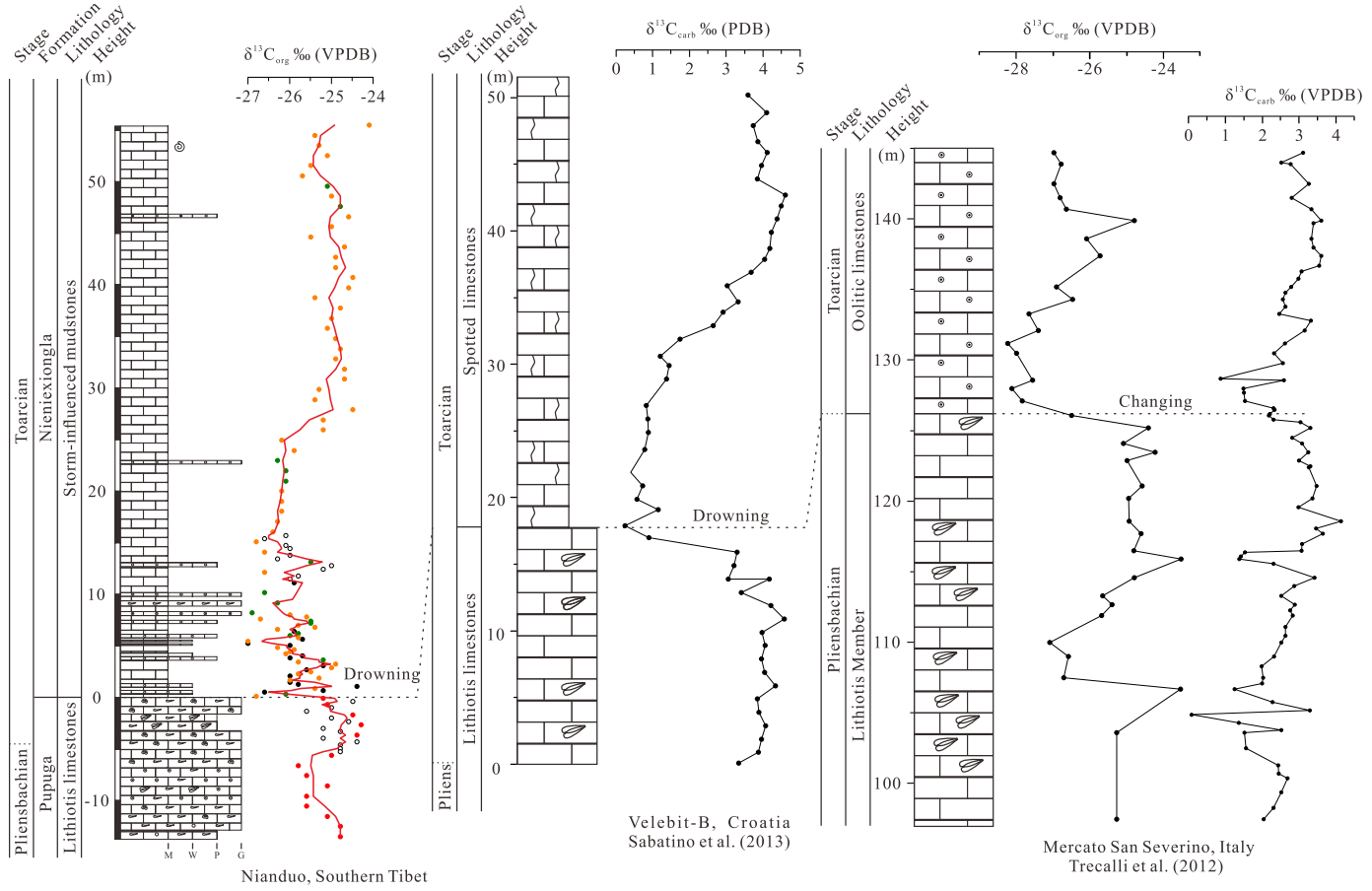

Fig. 7. Chemostratigraphic and lithological correlation of the Nianduo section with sections from the Adriatic Carbonate Platform in Croatia (Sabatino et al., 2013) and the Apennine Carbonate Platform in southern Italy (Trecalli et al., 2012). This correlation is based on the boundary of abrupt facies change from *Lithiotis* limestones to mudstones/oolitic limestones. This change is broadly consistent with the onset of the Toarcian CIE in each section.

effects (Dalrymple and Hoogendoorn, 1997). Gutter casts are generally attributed to powerful unidirectional currents created during the rising and peak phases of storms (Myrow and Southard, 1996). However, recent studies have shown that abundant occurrence of HCS/SCS within sandstone beds that infilled gutter casts indicates that gutter erosion and rapid subsequent infill can be ascribed to offshore-directed and oscillatory-dominant combined flows during storms (e.g., Collins et al., 2017). Therefore, the high-frequency gutter casts, HCS/SCS, and ripple marks in the studied sections clearly indicate the process of storms. Other abundant structures occurring in coarse-grained beds, like parallel laminations, climbing ripples, graded bedding and sharp erosive bases, are similar to those of turbidites formed under traction currents. However, these units cannot be clearly identified as turbidites in the Nianduo and Wölong sections because characteristic structures formed under unidirectional flow (flute casts and current ripples), as well as Bouma-style grading, were not observed.

Storm-related beds in the Nianduo and Wölong sections are abundant within the T-OAE interval, after maximum flooding at the Pupuga–Nieniexiongla boundary. Two earlier marine transgressions are recorded in Pliensbachian strata of the Pupuga Formation (Han et al., 2016), but storm deposits were not observed within these older transgressive sequences. This observation indicates that increased storm deposition/activity was independent of changes in sea level, but closely linked to the T-OAE. Similarly, geochemical and sedimentological data have emerged in recent years to indicate that many other tropical/subtropical zones over a latitudinal range of 18°N to 35°N in the northern hemisphere of the western Tethys were also influenced by frequent storm events within the T-OAE, as summarized by Krencker et al. (2015). These storm deposits are present in siliciclastic- and carbonate-dominated settings along the western Tethys, especially in deeper outer carbonate ramp and (hemi)pelagic environments (e.g., Suan et al., 2013; Pittet et al., 2014; Krencker et al., 2015; Han et al., 2016). Recent work by Izumi et al. (2018) has also demonstrated evidence of storm activity within the T-OAE in the shallow water margin of western Panthalassa. Thus, an enhanced intensity of storm events during the early Toarcian can be inferred that resulted in a basinward shift and deepening of effective storm wave base.

Two primary mechanisms can lead to deposition of storm beds: (1) winter storms and (2) tropical cyclones (Masselink and van Heteren, 2014). The common occurrence of storm-generated deposits in low latitudes (18–35°, Fig. 8) during the T-OAE excludes winter storms as the predominant phenomenon, because these are generated by disturbances at the boundary between warm tropical and cold polar air masses confined to mid- to high-latitudes (30–60°) (Masselink and van Heteren, 2014). By contrast, tropical cyclones are usually generated at low latitudes on both sides of the Equator by enthalpy flux from condensation of rising warm and moist air, which is essentially tied to elevated sea-surface temperature (>26.5 °C; Gray, 1968). Evidence from $\delta^{18}O$ data from brachiopods, belemnites and fish teeth from the western Tethys suggest that seawater temperature rose significantly across the T-OAE interval (4–7 °C, e.g., Gómez et al., 2008; Suan et al., 2010; Dera et al., 2011). These results support a cause-and-effect relationship between extreme warmth and increased tropical cyclones that resulted in widely distributed storm deposits along the western Tethyan margins, as suggested by Krencker et al. (2015). Recent

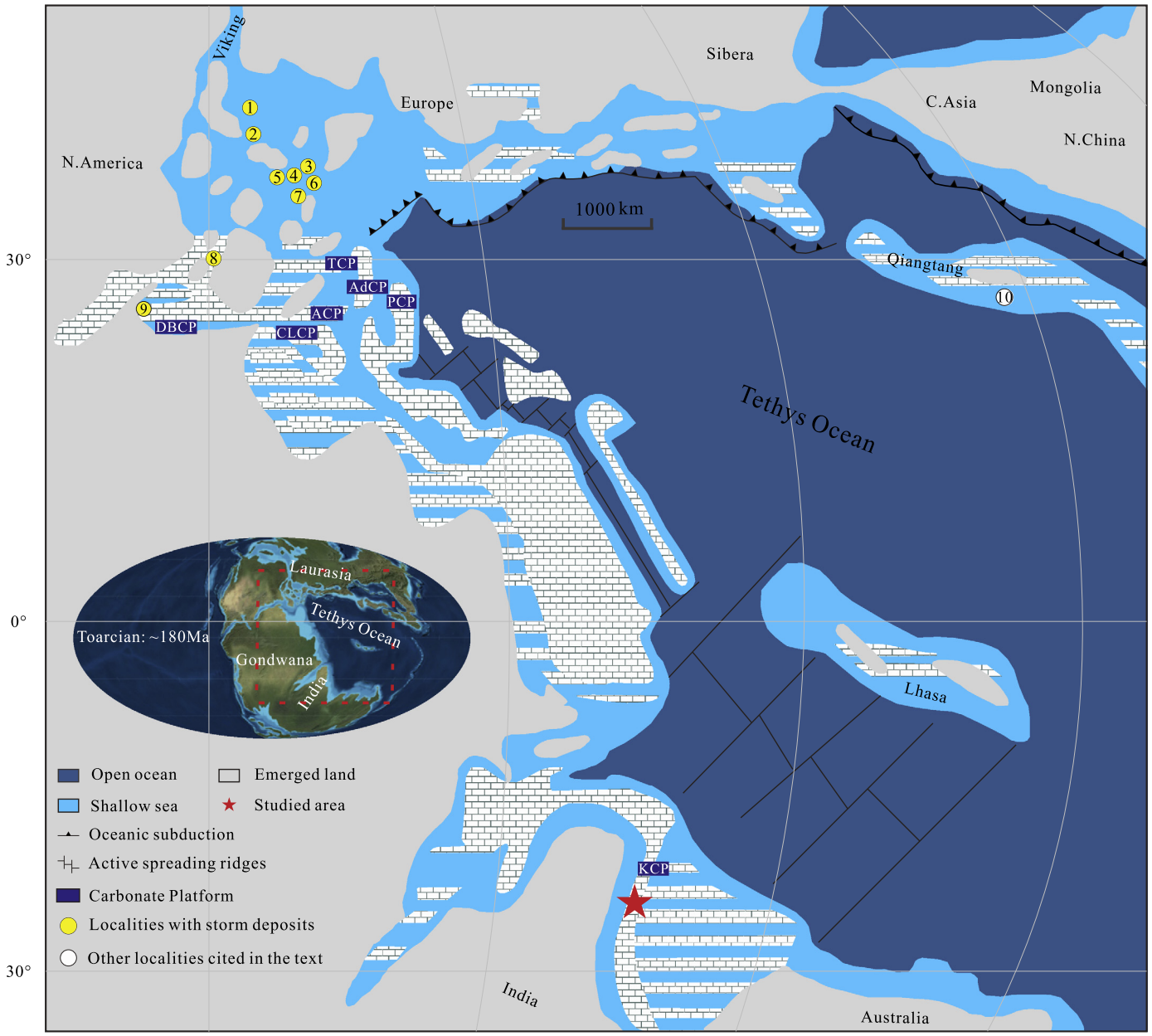

Fig. 8. (A) Palaeogeographic map of the Tethys Ocean during the Early Jurassic showing the key locations discussed in the text (modified after Golonka (2007) and Ron Blakey, http://jan.ucc.nau.edu/~rcb7/). The geographic distribution of storm deposits is modified after Krencker et al. (2015). 1 – Dutch Graben, Netherlands, 2 – Yorkshire, UK, 3 – Dotternhausen, SW Germany, 4 – Sancerre core, Paris Basin, France, 5 – ANDRA HTM-102 Borehole, NE France, 6 – Lafarge quarry, SE France, 7 – Causses Basin, Central-South France, 8 – Lusitanian basin, Portugal, 9 – Dades Valley, Morocco, 10 – Bilong Co, southern Qiangtang. TCP – Trento Carbonate Platform, AdCP – Adriatic Carbonate Platform, PCP – Pelagonian Carbonate Platform, ACP – Apennine Carbonate Platform, CLCP – Campania–Lucania Carbonate Platform, DBCP – Djebel Bou Dahar Carbonate Platform, KCP – Kioto Carbonate Platform.

climate models further confirm that elevated CO_2 concentration and sea-surface temperature can trigger more frequent and intense tropical cyclones, and also lead to a poleward expansion of storms (Emanuel, 2016; Korty et al., 2017).

5.4. Possible mechanisms for biotic carbonate-platform demise and delayed recovery during the early Toarcian

The correlation between the Tethyan carbonate-platform successions indicates that the top *Lithiotis* horizon in each section coincides with abrupt facies changes coincident with the onset of the $\delta^{13}C$ CIE and biotic platform demise by drowning or switching to non-skeletal carbonates (Fig. 7; Trecalli et al., 2012; Sabatino et al., 2013). Based on the chemostratigraphy and biostratigraphy, the late Pliensbachian–earliest Toarcian Kioto platform was a healthy carbonate platform dominated by hyper-productive massive mound-building bivalves (*Lithiotis* group), just like other tropical Tethyan and Panthalassan shallow-water carbonate platforms during the Early Jurassic (Fraser et al., 2004; Franceschi et al., 2014). The drowning of these platforms in the early Toarcian during the T-OAE was a regional, if not global, phenomenon. Notably, in the western Tethys (Fig. 8), the Pliensbachian–earliest Toarcian *Lithiotis* limestones of the NW Adriatic carbonate platform (Slovenia, central and western Croatia and western Bosnia) were directly overlain by early Toarcian dark spotted limestones (Vlahović et al., 2005; Sabatino et al., 2013), and deposits with abundant *Lithiotis* bivalves, sponge, and coral of the Djebel Bou Dahar platform were covered by Toarcian silty shale and limestones/marl alterna-

tions (Merino-Tomé et al., 2012). However, some platforms experienced transient drowning or shifted to an unfossiliferous platform type. The shallow-water carbonates rich in *Lithiotis* bivalves of the western Trento and Campania–Lucania platforms turned to clay-rich facies, and were locally replaced by crinoid-rich and unfossiliferous oolitic sediments, respectively (Woodfine et al., 2008). Several resilient platforms (Apennine and Pelagonian platforms, and the rest of NW Adriatic platform) changed from biotic platform type, dominated by *Lithiotis*/*P. mediterraneus*, to unfossiliferous oolitic platform (Vlahović et al., 2005; Scherreiks et al., 2010; Trecalli et al., 2012). These observations show that the demise of early Toarcian biotic platforms through either drowning or changing to fossil-scarce oolitic platforms was prevalent along the entire Tethyan tropical/subtropical realms (Fig. 8).

Some areas of the western Tethys were located in a relatively tectonically active area during the early Toarcian, and hence tectonic subsidence could be the major factor that led to drowning of some platforms (Lachkar et al., 2009; Merino-Tomé et al., 2012). However, this process alone was unlikely to have been a significant causal influence on Kioto platform drowning in the Tethyan Himalaya because the mature passive margin of northern India was relatively tectonically quiescent, with smooth reconstructed subsidence curves through the early Jurassic (Sciunnach and Garzanti, 2012). Several meters of sea-level rise occurred during the early Toarcian at the *tenuicostatum* (*antiquum*)–*falciferum* zone transition (Suan et al., 2010, 2011). Nevertheless, for a healthy and highly productive platform, carbonate production should have been fast enough to keep up with this rise (Schlager, 1981; Godet, 2013).

A number of key palaeoenvironmental factors, such as nutrient excesses, anoxic/suboxic conditions, acidification, clastic delivery, elevated temperature, or a combination of these, have been suggested as potential triggering mechanisms for drowning of carbonate platforms in the geological record (Godet, 2013). Importantly, within the resolution of the $\delta^{13}C$ data, the extensive biotic platform drowning or shifting to fossil-scarce oolitic platform occurs across the first phase of the T-OAE CIE, i.e., just before minimum isotopic values are reached (Fig. 7). The environmental deterioration of the global ocean associated with the likely large-scale release of carbon into the ocean–atmosphere system most probably led to extensive biotic platform demise. The T-OAE was associated with increased continental discharge and nutrient input (Cohen et al., 2004; Jenkyns, 2010; Brazier et al., 2015; Izumi et al., 2018). However, deeper marine shales and siltstones representing clastic input and phosphatic hardgrounds reflecting eutrophic conditions are not observed on the top of the drowning unconformity on the eastern Tethyan Kioto platform. According to detailed microfaceies analysis by Han et al. (2016) and our Ti data (Fig. 3), the shallow-marine carbonates are mainly overlain by lime mudstones (0–6 m) and the level of the first clastic-rich unit occurs 0.4 m above the drowning boundary. These facts indicate that there was no immediate increase in clastic delivery and nutrient input when the Kioto platform drowned. The proxies mentioned above reflecting increased clastic and nutrient input were also not reported at the boundary of the facies change in the western Tethyan Apennine and Adriatic platforms in the early Toarcian (Trecalli et al., 2012; Sabatino et al., 2013). Therefore, enhanced clastic input and subsequent eutrophication are unlikely to explain the entire Tethyan platform demise in the early Toarcian. Oxygen-depleted conditions likely influenced numerous Tethyan continental margins, because box-modeling of sulfur isotope changes suggest that pyrite burial in the NW Tethys alone could not explain the positive $\delta^{34}S$ excursion (Gill et al., 2011). However, the mean framboid diameter distribution (5.96–8.35 μm) on the Kioto platform (Wignall et al., 2006) and the manganese chemostratigraphy on the Adriatic carbonate platform (Sabatino et al., 2013) suggests a sudden change from oxygen-rich to relatively lower dissolved oxygen contents in the bottom waters, which could have played a role in the abrupt demise of the Tethyan carbonate platforms. Ocean acidification also has been invoked to explain the demise of biotic platforms at the onset of the T-OAE because the prolific *Lithiotis*/*P. mediterraneus* are expected to be vulnerable to a reduction of carbonate saturation caused by a dramatic decrease of pH (Trecalli et al., 2012). This hypothesis seems to be reasonable on the basis of the estimated mass and rate of carbon release during the T-OAE (McElwain et al., 2005). As discussed above, extreme warmth likely prevailed along the entire tropical/subtropical Tethys through the T-OAE. Recent studies further show that a significant increase in seawater temperature, around the *tenuicostatum*–*falciferum* zone boundary of early Toarcian age, marks the mass extinction level (Gómez et al., 2008; Gómez and Goy, 2011). Thus, warming that possibly combined with oceanic acidification and slight oxygen depletion, likely led to mass extinction of benthic fauna and biotic carbonate-platform drowning/changing to a non-skeletal platform.

As mentioned above, after the early Toarcian biocalcification crisis, several resilient platforms of the western Tethys quickly changed from biotic platforms, dominated by *Lithiotis*/*P. mediterraneus*, to unfossiliferous oolitic platforms, probably due to the rapid rebound of carbonate supersaturation in shallow marine environments (Vlahović et al., 2005; Scherreiks et al., 2010; Trecalli et al., 2012). If other conditions were favorable, the rapid recovery of ocean alkalinity and carbonate saturation should have promoted the thriving of biotic platforms, while unfossiliferous oolitic platforms developed extensively. Consequently, after the T-OAE biotic crisis, extreme warmth seems to have been the major factor that suppressed and postponed the recovery of biotic platforms dominated by reef-building corals or bivalves. Such a rapid and persistent warming could have triggered a severe biotic crisis, and was contemporaneously beneficial to calcium carbonate precipitation, which further facilitated the wide distribution of non-skeletal platforms in shallow settings with carbonate-supersaturated seawater. Therefore, extreme and persistent warming conditions can reasonably explain the coexistent and prevalent pattern of biotic platform demise by shifting to unfossiliferous oolitic platforms/drowning in shallow/relative deeper settings with/without carbonate-supersaturated seawater along the entire Tethys.

6. Conclusions

This study reports T-OAE records from a carbonate platform exposed in the Tibetan Himalaya, and originally deposited on the open SE Tethyan margin of the southern hemisphere. Based on new biostratigraphical, geochemical and sedimentological data, we have reconstructed palaeoenvironmental and palaeoclimatic changes of the northern Indian margin through the late Pliensbachian–early Toarcian interval, encompassing the T-OAE. $\delta^{13}C_{org}$ data from the Nianduo succession of this platform delineates the T-OAE CIE with a magnitude of $-2.5‰$, but a CIE with a reduced magnitude of $-1.5‰$ is present in $\delta^{13}C_{carb}$ data. The Wölong succession illustrates only a recovery trend in $\delta^{13}C_{org}$ data, and not a clear CIE.

The common occurrence of storm deposits likely associated with tropical weather systems indicates that the well-established and marked global warming during the T-OAE severely influenced the eastern Tethyan margin. This feature of both the Nianduo and Wölong sections is similar to the observations of storm deposits made in the western Tethys of the northern hemisphere by Krencker et al. (2015), who also linked such storms to climate warming. The extreme warm conditions, in response to carbon release during the T-OAE, likely played a key role in the observed sudden biotic platform demise recorded in our Tibetan sections, and also observed across the wider tropical/subtropical Tethys. Af-

ter the onset of the early Toarcian CIE, ocean alkalinity and carbonate saturation might have quickly recovered from the oceanic acidification, leading to conditions favorable for the extensive development of non-skeletal platforms in shallow waters (Trecalli et al., 2012). Nevertheless, the persistence of extreme warm conditions through the early Toarcian could have suppressed and postponed the redevelopment of biotic platforms dominated by reef-building bivalves and/or corals.

Acknowledgements

We are grateful to Zhifei Liu for TOC and $\delta^{13}C_{carb}$ analyses at the Tongji University. We thank also Wei An, Bo Zhou and Shiyi Li for their assistance in the field, and Zhicheng Huang, Yiwei Xu and Weiwei Xue for their help in the laboratory, and Chao Chang, Tianchen He and Bolin Zhang for their helpful discussion. Hugh Jenkyns commented on a draft of the manuscript. We would also like to thank Editor Derek Vance, Christopher Pearce and two anonymous reviewers whose comments greatly improved the manuscript. This study was financially supported by the National Natural Science Funds for Distinguished Young Scholar in China (41525007) and the Chinese MOST 973 Project (2012CB822001). DBK acknowledges support of NERC Fellowship NE/I02089X/1. This is a contribution to the IGCP 655.

Appendix A. Supplementary material

Supplementary material related to this article can be found online at https://doi.org/10.1016/j.epsl.2018.02.017.

References

Al-Suwaidi, A.H., Angelozzi, G.N., Baudin, F., Damborenea, S.E., Hesselbo, S.P., Jenkyns, H.C., Mancenido, M.O., Riccardi, A.C., 2010. First record of the Early Toarcian Oceanic Anoxic Event from the Southern Hemisphere, Neuquen Basin, Argentina. J. Geol. Soc. Lond. 167, 633–636.

Al-Suwaidi, A.H., Hesselbo, S.P., Damborenea, S.E., Mancenido, M.O., Jenkyns, H.C., Riccardi, A.C., Angelozzi, G.N., Baudin, F., 2016. The Toarcian Oceanic Anoxic Event (Early Jurassic) in the Neuquen Basin, Argentina: a reassessment of age and carbon isotope stratigraphy. J. Geol. 124, 171–193.

Bodin, S., Krencker, F.N., Kothe, T., Hoffmann, R., Mattioli, E., Heimhofer, U., Kabiri, L., 2016. Perturbation of the carbon cycle during the late Pliensbachian–early Toarcian: new insight from high-resolution carbon isotope records in Morocco. J. Afr. Earth Sci. 116, 89–104.

BouDagher-Fadel, M.K., 2008. Evolution and Geological Significance of Larger Benthic Foraminifera, vol. 404. Elsevier, Amsterdam, pp. 1–544.

Brasier, M.D., Magaritz, M., Corfield, R., Huilin, L., Xiche, W., Lin, O., Zhiwen, J., Hamdi, B., Tinggui, H., Fraser, A., 1990. The carbon and oxygen isotope record of the Precambrian–Cambrian boundary interval in China and Iran and their correlation. Geol. Mag. 127, 319–332.

Brazier, J.M., Suan, G., Tacail, T., Simon, L., Martin, J.E., Mattioli, E., Baiter, V., 2015. Calcium isotope evidence for dramatic increase of continental weathering during the Toarcian oceanic anoxic event (Early Jurassic). Earth Planet. Sci. Lett. 411, 164–176.

Caruthers, A.H., Grocke, D.R., Smith, P.L., 2011. The significance of an Early Jurassic (Toarcian) carbon-isotope excursion in Haida Gwaii (Queen Charlotte Islands), British Columbia, Canada. Earth Planet. Sci. Lett. 307, 19–26.

Cohen, A.S., Coe, A.L., Harding, S.M., Schwark, L., 2004. Osmium isotope evidence for the regulation of atmospheric CO_2 by continental weathering. Geology 32, 157–160.

Collins, D.S., Johnson, H.D., Allison, P.A., Guilpain, P., Damit, A.R., 2017. Coupled 'storm-flood' depositional model: application to the Miocene—Modern Baram Delta Province, North-West Borneo. Sedimentology 64, 1203–1235.

Dalrymple, R.W., Hoogendoorn, E.L., 1997. Erosion and deposition on migrating shoreface-attached ridges, Sable Island, eastern Canada. Geosci. Can. 24, 25–36.

Dera, G., Brigaud, B., Monna, F., Laffont, R., Puceat, E., Deconinck, J.F., Pellenard, P., Joachimski, M.M., Durlet, C., 2011. Climatic ups and downs in a disturbed Jurassic world. Geology 39, 215–218.

Emanuel, K., 2016. Will global warming make hurricane forecasting more difficult? Bull. Am. Meteorol. Soc., 495–501.

Fichtner, V., Strauss, H., Immenhauser, A., Buhl, D., Neuser, R.D., Niedermayr, A., 2017. Diagenesis of carbonate associated sulfate. Chem. Geol. 463, 61–75.

Franceschi, M., Dal Corso, J., Posenato, R., Roghi, G., Masetti, D., Jenkyns, H.C., 2014. Early Pliensbachian (Early Jurassic) C-isotope perturbation and the diffusion of the Lithiotis Fauna: insights from the western Tethys. Palaeogeogr. Palaeoclimatol. Palaeoecol. 410, 255–263.

Fraser, N.M., Bottjer, D.J., Fischer, A.G., 2004. Dissecting "Lithiotis" bivalves: implications for the Early Jurassic reef eclipse. Palaios 19, 51–67.

Fu, X., Wang, J., Feng, X., Wang, D., Chen, W., Song, C., Zeng, S., 2016. Early Jurassic carbon-isotope excursion in the Qiangtang Basin (Tibet), the eastern Tethys: implications for the Toarcian Oceanic anoxic event. Chem. Geol. 442, 62–72.

Gansser, 1964. Geology of the Himalayas. Interscience Publishers, John Wiley and Sons, New York (289 pp.).

Gill, B.C., Lyons, T.W., Jenkyns, H.C., 2011. A global perturbation to the sulfur cycle during the Toarcian Oceanic Anoxic Event. Earth Planet. Sci. Lett. 312, 484–496.

Godet, A., 2013. Drowning unconformities: palaeoenvironmental significance and involvement of global processes. Sediment. Geol. 293, 45–66.

Golonka, J., 2007. Phanerozoic paleoenvironment and paleolithofacies maps. Mesozoic. Geologia 35, 589–654.

Gómez, J.J., Goy, A., 2011. Warming-driven mass extinction in the Early Toarcian (Early Jurassic) of northern and central Spain. Correlation with other time-equivalent European sections. Palaeogeogr. Palaeoclimatol. Palaeoecol. 306, 176–195.

Gómez, J.J., Goy, A., Canales, M.L., 2008. Seawater temperature and carbon isotope variations in belemnites linked to mass extinction during the Toarcian (Early Jurassic) in Central and Northern Spain. Comparison with other European sections. Palaeogeogr. Palaeoclimatol. Palaeoecol. 258, 28–58.

Gray, W.M., 1968. Global view of the origin of tropical disturbances and storms. Mon. Weather Rev. 96, 669–900.

Gröcke, D.R., Hori, R.S., Trabucho-Alexandre, J., Kemp, D.B., Schwark, L., 2011. An open ocean record of the Toarcian oceanic anoxic event. Solid Earth 2, 245–257.

Han, Z., Hu, X.M., Li, J., Garzanti, E., 2016. Jurassic carbonate microfacies and relative sea-level changes in the Tethys Himalaya (southern Tibet). Palaeogeogr. Palaeoclimatol. Palaeoecol. 456, 1–20.

Hermoso, M., Le Callonnec, L., Minoletti, F., Renard, M., Hesselbo, S.P., 2009. Expression of the Early Toarcian negative carbon-isotope excursion in separated carbonate microfractions (Jurassic, Paris Basin). Earth Planet. Sci. Lett. 277, 194–203.

Hermoso, M., Minoletti, F., Rickaby, R.E.M., Hesselbo, S.P., Baudin, F., Jenkyns, H.C., 2012. Dynamics of a stepped carbon-isotope excursion: ultra high-resolution study of Early Toarcian environmental change. Earth Planet. Sci. Lett. 319, 45–54.

Hesselbo, S.P., Grocke, D.R., Jenkyns, H.C., Bjerrum, C.J., Farrimond, P., Morgans Bell, H.S., 2000. Massive dissociation of gas hydrate during a Jurassic oceanic anoxic event. Nature 406, 392–395.

Hesselbo, S.P., Jenkyns, H.C., Duarte, L.V., Oliveira, L.C.V., 2007. Carbon-isotope record of the Early Jurassic (Toarcian) Oceanic Anoxic Event from fossil wood and marine carbonate (Lusitanian Basin, Portugal). Earth Planet. Sci. Lett. 253, 455–470.

Hesselbo, S.P., Pieńkowski, G., 2011. Stepwise atmospheric carbon-isotope excursion during the Toarcian Oceanic Anoxic Event (Early Jurassic, Polish Basin). Earth Planet. Sci. Lett. 301, 365–372.

Huang, W.T., van Hinsbergen, D.J., Dekkers, M.J., Garzanti, E., Dupont-Nivet, G., Lippert, P.C., Li, X.C., Maffione, M., Langereis, C.G., Hu, X.M., 2015. Paleolatitudes of the Tibetan Himalaya from primary and secondary magnetizations of Jurassic to Lower Cretaceous sedimentary rocks. Geochem. Geophys. Geosyst. 16, 77–100.

Izumi, K., Kemp, D.B., Itamiya, S., Inui, M., 2018. Sedimentary evidence for enhanced hydrological cycling in response to rapid carbon release during the early Toarcian oceanic anoxic event. Earth Planet. Sci. Lett. 481, 162–170.

Jadoul, F., Berra, F., Garzanti, E., 1998. The Tethys Himalayan passive margin from Late Triassic to Early Cretaceous (South Tibet). J. Asian Earth Sci. 16, 173–194.

Jenkyns, H.C., 1988. The early Toarcian (Jurassic) anoxic event, stratigraphic, sedimentary and geochemical evidence. Am. J. Sci. 288, 101–151.

Jenkyns, H.C., 2010. Geochemistry of oceanic anoxic events. Geochem. Geophys. Geosyst. 11, 1–30.

Jenkyns, H.C., Jones, C.E., Grocke, D.R., Hesselbo, S.P., Parkinson, D.N., 2002. Chemostratigraphy of the Jurassic system: applications, limitations and implications for palaeoceanography. J. Geol. Soc. Lond. 159, 351–378.

Kaufman, A.J., Knoll, A.H., 1995. Neoproterozoic variations in the C-isotopic composition of seawater: stratigraphic and biogeochemical implications. Precambrian Res. 73, 27–49.

Kemp, D.B., Coe, A.L., Cohen, A.S., Schwark, L., 2005. Astronomical pacing of methane release in the Early Jurassic period. Nature 437, 396–399.

Kemp, D.B., Izumi, K., 2014. Multiproxy geochemical analysis of a Panthalassic margin record of the early Toarcian oceanic anoxic event (Toyora area, Japan). Palaeogeogr. Palaeoclimatol. Palaeoecol. 414, 332–341.

Knoll, A.H., Hayes, J.M., Kaufman, A.J., Swett, K., Lambert, I.B., 1986. Secular variation in carbon isotope ratios from Upper Proterozoic successions of Svalbard and East Greenland. Nature 321, 832–838.

Korty, R.L., Emanuel, K.A., Huber, M., Zamora, R.A., 2017. Tropical cyclones downscaled from simulations with very high carbon dioxide levels. J. Climate 30, 649–667.

Krencker, F.N., Bodin, S., Suan, G., Heimhofer, U., Kabiri, L., Immenhauser, A., 2015. Toarcian extreme warmth led to tropical cyclone intensification. Earth Planet. Sci. Lett. 425, 120–130.

Lachkar, N., Guiraud, M., El Harfi, A., Dommergues, J.L., Dera, G., Durlet, C., 2009. Early Jurassic normal faulting in a carbonate extensional basin: characterization of tectonically driven platform drowning (High Atlas rift, Morocco). J. Geol. Soc. Lond. 166, 413–430.

Littler, K., Hesselbo, S.P., Jenkyns, H.C., 2010. A carbon-isotope perturbation at the Pliensbachian–Toarcian boundary: evidence from the Lias Group, NE England. Geol. Mag. 147, 181–192.

Liu, G.H., Einsele, G., 1994. Sedimentary history of the Tethyan basin in the Tibetan Himalayas. Geol. Rundsch. 83, 32–61.

Masselink, G., van Heteren, S., 2014. Response of wave-dominated and mixed-energy barriers to storms. Mar. Geol. 352, 321–347.

McElwain, J.C., Wade-Murphy, J., Hesselbo, S.P., 2005. Changes in carbon dioxide during an oceanic anoxic event linked to intrusion into Gondwana coals. Nature 435, 479–482.

Merino-Tomé, O., Della Porta, G., Kenter, J.A.M., Verwer, K., Harris, P., Adams, E.W., Playton, T., Corrochano, D., 2012. Sequence development in an isolated carbonate platform (Lower Jurassic, Djebel Bou Dahar, High Atlas, Morocco): influence of tectonics, eustacy and carbonate production. Sedimentology 59, 118–155.

Myrow, P.M., Southard, J.B., 1996. Tempestite deposition. J. Sediment. Res. 66, 875–887.

Newton, R.J., Reeves, E.P., Kafousia, N., Wignall, P.B., Bottrell, S.H., Sha, J.-G., 2011. Low marine sulfate concentrations and the isolation of the European epicontinental sea during the Early Jurassic. Geology 39, 7–10.

Oehlert, A.M., Swart, P.K., 2014. Interpreting carbonate and organic carbon isotope covariance in the sedimentary record. Nat. Commun. 5, 4672.

Pearce, C.R., Cohen, A.S., Coe, A.L., Burton, K.W., 2008. Molybdenum isotope evidence for global ocean anoxia coupled with perturbations to the carbon cycle during the Early Jurassic. Geology 36, 231–234.

Pittet, B., Suan, G., Lenoir, F., Duarte, L.V., Mattioli, E., 2014. Carbon isotope evidence for sedimentary discontinuities in the lower Toarcian of the Lusitanian Basin (Portugal): sea level change at the onset of the Oceanic Anoxic Event. Sediment. Geol. 303, 1–14.

Sabatino, N., Vlahovic, I., Jenkyns, H.C., Scopelliti, G., Neri, R., Prtoljan, B., Velic, I., 2013. Carbon-isotope record and palaeoenvironmental changes during the early Toarcian oceanic anoxic event in shallow-marine carbonates of the Adriatic Carbonate Platform in Croatia. Geol. Mag. 150, 1085–1102.

Scherreiks, R., Bosence, D., BouDagher-Fadel, M., Meléndez, G., Baumgartner, P.O., 2010. Evolution of the Pelagonian carbonate platform complex and the adjacent oceanic realm in response to plate tectonic forcing (Late Triassic and Jurassic), Evvoia, Greece. Int. J. Earth Sci. (Geol. Rundsch.) 99, 1317–1334.

Schlager, W., 1981. The paradox of drowned reefs and carbonate platforms. Geol. Soc. Am. Bull. 92, 197–211.

Sciunnach, D., Garzanti, E., 2012. Subsidence history of the Tethys Himalaya. Earth-Sci. Rev. 111, 179–198.

Suan, G., Mattioli, E., Pittet, B., Lecuyer, C., Sucheras-Marx, B., Duarte, L.V., Philippe, M., Reggiani, L., Martineau, F., 2010. Secular environmental precursors to Early Toarcian (Jurassic) extreme climate changes. Earth Planet. Sci. Lett. 290, 448–458.

Suan, G., Nikitenko, B.L., Rogov, M.A., Baudin, F., Spangenberg, J.E., Knyazev, V.G., Glinskikh, L.A., Goryacheva, A.A., Adatte, T., Riding, J.B., Follmi, K.B., Pittet, B., Mattioli, E., Lecuyer, C., 2011. Polar record of Early Jurassic massive carbon injection. Earth Planet. Sci. Lett. 312, 102–113.

Suan, G., Rulleau, L., Mattioli, E., Sucheras-Marx, B., Rousselle, B., Pittet, B., Vincent, P., Martin, J.E., Lena, A., Spangenberg, J.E., Follmi, K.B., 2013. Palaeoenvironmental significance of Toarcian black shales and event deposits from southern Beaujolais, France. Geol. Mag. 150, 728–742.

Suan, G., van de Schootbrugge, B., Adatte, T., Fiebig, J., Oschmann, W., 2015. Calibrating the magnitude of the Toarcian carbon cycle perturbation. Paleoceanography 30, 495–509.

Them, T., Gill, B., Caruthers, A., Gröcke, D., Tulsky, E., Martindale, R., Poulton, T., Smith, P., 2017. High-resolution carbon isotope records of the Toarcian Oceanic Anoxic Event (Early Jurassic) from North America and implications for the global drivers of the Toarcian carbon cycle. Earth Planet. Sci. Lett. 459, 118–126.

Trecalli, A., Spangenberg, J., Adatte, T., Follmi, K.B., Parente, M., 2012. Carbonate platform evidence of ocean acidification at the onset of the early Toarcian oceanic anoxic event. Earth Planet. Sci. Lett. 357, 214–225.

van de Schootbrugge, B., McArthur, J.M., Bailey, T.R., Rosenthal, Y., Wright, J.D., Miller, K.G., 2005. Toarcian oceanic anoxic event: an assessment of global causes using belemnite C isotope records. Paleoceanography 20, PA3008.

Vlahović, I., Tisljar, J.I., Maticec, D., 2005. Evolution of the Adriatic Carbonate Platform: palaeogeography, main events and depositional dynamics. Palaeogeogr. Palaeoclimatol. Palaeoecol. 220, 333–360.

Wignall, P.B., Hallam, A., Newton, R.J., Sha, J.G., Reeves, E., Mattioli, E., Crowley, S., 2006. An eastern Tethyan (Tibetan) record of the Early Jurassic (Toarcian) mass extinction event. Geobiology 4, 179–190.

Woodfine, R.G., Jenkyns, H.C., Sarti, M., Baroncini, F., Violante, C., 2008. The response of two Tethyan carbonate platforms to the early toarcian (Jurassic) oceanic anoxic event: environmental change and differential subsidence. Sedimentology 55, 1011–1028.

Xu, W., Ruhl, M., Jenkyns, H., Hesselbo, S., Riding, J., Selby, D., Naafs, B., Weijers, J., Pancost, R., Tegelaar, E., 2017. Carbon sequestration in an expanding lake system during the Toarcian Oceanic Anoxic Event. Nat. Geosci. 10, 129–135.

Yin, J.R., 2010. Jurassic Ammonites of Tibet. Geological Publishing House, Beijing (247 pp.; in Chinese with English abstract).